Mon. Not. R. Astron. Soc. **000**, 1–5 (2022) Printed 22 September 2023 (MN LATEX style file v2.2)

Interface of Equation-of-State, Atomic Data and Opacities in the Solar Problem

Anil K. Pradhan[1,2]
[1] *Department of Astronomy,* [2] *Chemical Physics Program, The Ohio State University, Columbus, OH 43210, USA.*

Accepted xxxxxx Received xxxxxx; in original form xxxxxx

ABSTRACT

Convergence of the Rosseland Mean Opacity (RMO) is investigated with respect to the equation-of-state (EOS) and the number of atomic levels of iron ions prevalent at the solar radiative/convection boundary. The "chemical picture" Mihalas-Hummer-Däppen MHD-EOS, and its variant QMHD-EOS, are studied at two representative temperature-density sets at the base of the convection zone (BCZ) and the Sandia Z experiment: $(2 \times 10^6 K,\ 10^{23}/cc)$ and $(2.11 \times 10^6 K,\ 3.16 \times 10^{22}/cc)$, respectively. It is found that whereas the new atomic datasets from accurate R-matrix calculations for opacities (RMOP) are vastly overcomplete, involving hundreds to over a thousand levels of each of the three Fe ions considered — Fe XVII , Fe XVIII , Fe XIX — the EOS constrains contributions to RMOs by relatively fewer levels. The RMOP iron opacity spectrum is quite different from the Opacity Project distorted wave model and shows considerably more plasma broadening effects. This work points to possible improvements needed in the EOS for opacities in high-energy-density (HED) plasma sources.

Key words: Physical Data and Processes, atomic processes

1 INTRODUCTION

As a fundamental quantity in light-matter interaction opacity plays a key role in astrophysics, such as stellar interiors, helioseismology, and asteroseimology, elemental abundance determination, host-star and exoplanetary fluxes, etc. (Christensen-Dalsgaard *et al.* (2009); Basu *et al.* (2015); Asplund *et al.* (2009); Carlos *et al.* (2019); Buldgen *et al.* (2023a). In addition, radiation transport models of inertial plasma fusion devices requires accurate opacities (Bailey *et al.* (2015); Perry *et al.* (2018). In particular, the outstanding uncertainty in the solar chemical composition affects elemental calibration of all astronomical sources. Attempts to employ advances in helioseismology and abundances are an active area of basic research (Basu and Antia (2008); Buldgen *et al.* (2022), but require enhanced solar opacities by about 10%. That, in turn, depends on two elements, oxygen and iron, that determine about half of the solar opacity at BCZ. However, a downward revision of oxygen abundance by up to 20-40% from earlier solar composition is a major part of the "solar problem" (Asplund *et al.* (2021); Pietrow *et al.* (2023); Li *et al.* (2023); Buldgen *et al.* (2023b). Since about 90% of oxygen is either fully ionized or H-like at BCZ, its absorption coefficient is small and unlikely to change from current atomic calculations, enhanced iron opacity might countenance lower solar abundances (Bailey *et al.* (2015).

Opacity computations depend on atomic data on the one hand and the plasma EOS on the other (The Opacity Project Team (1995); Seaton *et al.* (1994); Pradhan *et al.* (2023). Voluminous amounts of data are needed for all photon absorption and scattering processes in order to ensure completeness. Recently, accurate and extensive calculations of atomic data for iron ions of importance under BCZ conditions have been carried out using the R-matrix method (Pradhan *et al.* (2023); Nahar *et al.* (2023); Pradhan (2023); Zhao *et al.* (2023). However, the EOS determines how and to what extent the atomic data contribute to monochromatic and mean opacities at a given temperature and density. The Planck and Rosseland Mean Opacity (PMO and RMO respectively) are defined as

$$\kappa_P B(T) = \int \kappa_\nu B_\nu d\nu, \tag{1}$$

$$\frac{1}{\kappa_R} = \frac{\int_0^\infty g(u)\kappa_\nu^{-1} du}{\int_0^\infty g(u) du} \quad ; \quad g(u) = u^4 e^{-u}(1-e^{-u})^{-2}, \tag{2}$$

where $g(u) = dB_\nu/dT$ is the derivative of the Planck weighting function

$$B_\nu(T) = \frac{(2h\nu^3/c^2)}{e^{h\nu/kT} - 1} \tag{3}$$

,

and κ_ν is the monochromatic opacity. Atomic processes and contributions to opacity are from bound-bound (bb), bound-free (bf), free-free (ff), and photon scattering (sc) as

$$\kappa_{ijk}(\nu) = \sum_k a_k \sum_j x_j \sum_{i,i'} [\kappa_{bb(}(i,i';\nu) \quad (4)$$

$$+ \kappa_{bf}(i,\epsilon i';\nu) + \kappa_{ff}(\epsilon i,\epsilon' i';\nu) + \kappa_{sc}(\nu)] \ , \quad (5)$$

where a_k is the abundance of element k, x_j the j ionization fraction, i and i' are the initial bound and final bound/continuum states of the atomic species, and ϵ represents the electron energy in the continuum. Whereas the ff and sc contributions are small, the opacity is primarily governed by bb and bf atomic data that need to be computed for all atomic species. Existing opacity models generally employ the relatively simple distorted wave (DW) approximation based on atomic structure codes, but higher accuracy requires considerable effort.

Originally, the Opacity Project (The Opacity Project Team (1995) (hereafter OP) envisaged using the poweful and highly accurate R-matrix method for improved accuracy. But that turned out to be intractable owing to computational constraints, and also required theoretical developments related to relativistic fine structure and plasma broadening effects. Therefore, the OP opacities were finally computed using similar atomic physics as other existing opacity models, mainly based on the simpler distorted wave (DW) approximation (Seaton OPCD (2003), and later archived in the online database OPserver (Mendoza *et al.* (2007). However, following several developments since then renewed R-matrix calculations can now be carried out, as discussed below.

2 THEORETICAL FRAMEWORK

Recently, with several improvements in the extended R-matrix and opacity codes large-scale data have been computed for Fe ions Fe XVII , Fe XVIII and Fe XIX , which determine over 80% of iron opacity near BCZ conditions (Pradhan *et al.* (2023); Nahar *et al.* (2023); Pradhan (2023); Zhao *et al.* (2023). The R-matrix (RM) framework and comparison with existing opacity models based on atomic structure codes and the distorted wave (DW) approximation, and associated physical effects, are described in detail. The primary difference between the RM and DW approximations is the treatment of bound-free opacity which is dominated by autoionizing resonances that are included in an *ab initio* manner in RM calculations, but treated perturbatively as bound-bound transitions in the DW method. Plasma broadening effects are very important, but manifest themselves quite differently in the two methods. Resonances in RM photoionization cross sections are broadened far more than lines as function of temperature and density since autoionization widths, shapes and heights are considered explicitly (Pradhan (2023). Also, the intrinsically asymmetric features of the large Seaton photoexcitation-of-core (PEC) resonances in bound-free cross sections are preserved in RM calculations. The unverified assertion that RM and DW opacities are equivalent is incorrect owing to basic physical effects (Delahaye *et al.* (2021). On the contrary, the RM method is based on the coupled channel approximation that gives rise to autoionizing resonances, and has historically superseded the DW method which neglects channel coupling. RM calculations for all relevant atomic processes are generally much more accurate than the DW, as for example in the work carried out under the Iron Project, including relativistic effects in the Breit-Pauli R-matrix (BPRM) approximation (Hummer *et al.* (1993) that is also employed in the present work (Nahar *et al.* (2023).

The interface of atomic data with EOS parameters is implemented through the MHD-EOS (Mihalas *et al.* (1988), formulated in the "chemical picture" as designed for OP work. It is based on the concept of *occupation probability* w of an atomic level being populated in a plasma environment, characterized by a temperature-density (hereafter T-D) related to Boltzmann-Saha equations. The level population is then given as

$$N_{ij} = \frac{N_j g_{ij} w_{ij} e^{-E_{ij}/kT}}{U_j}, \quad (6)$$

where w_{ij} are the occupation probabilities of levels i in ionization state j, and U_j is the atomic internal partition function. The occupation probabilities do not have a sharp cut-off, but approach zero for high-n as they are "dissolved" due to plasma interactions. The partition function is re-defined as

$$U_j = \sum_i g_{ij} w_{ij} e^{(-E_{ij}/kT)}. \quad (7)$$

E_{ij} is the excitation energy of level i, g_{ij} its statistical weight, and T the temperature. The w_{ij} are determined upon free-energy minimization in the plasma at a given T-D. However, the original MHD-EOS was found to yield w-values that were unrealistically low by up to several orders of magnitude. An improved treatment of microfield distribution and plasma correlations was developed, leading to the so-called QMHD-EOS (Nayfonov *et al.* (1999) and employed for subsequent OP calculations and results (Seaton OPCD (2003); Mendoza *et al.* (2007).

3 OPACITY COMPUTATIONS

The new RMOP data are interfaced with the (Q)MHD-EOS to obtain opacities. Computed RM atomic data for bb oscillator strengths and bf photoionization cross sections of all levels up to n (SLJ) = 10 yields datasets for 454 levels for Fe XVII , 1174 levels for Fe XVIII and 1626 for Fe XIX (Nahar *et al.* (2023); some results for Fe XVII were reported earlier (Nahar and Pradhan (2016). Monochromatic and mean opacities may then be computed using atomic data for *any number of these levels and the EOS*.

In order to study the behavior of MHD and QMHD, we employ the new RMOP opacity codes (Pradhan *et al.* (2023), varying the number of atomic levels for each Fe ion, and both sets of EOS parameters at specified temperature-density pairs for a particular ion. Monochromatic opacities are computed at the same frequency mesh in the variable and range $0 \leqslant u = h\nu/kT \leqslant 20$, as in OP work (Seaton *et al.* (1994); Mendoza *et al.* (2007). Since RMOP calculations were carried out for the three Fe ions that comprise over 80% of total Fe at BCZ, we replace their opacity

spectra in OP codes (Seaton OPCD (2003) and recompute RMOP iron opacities. Thus, ∼15% contribution is from OP data for other Fe ions; a table of Fe ion fractions at BCZ is given in (Pradhan *et al.* (2023).

To circumvent apparently unphysical behavior of MHD-EOS at very high densities, an ad hoc occupation probability cut-off was introduced in OP calculations with $w(i) \geqslant 0.001$ (Badnell and Seaton (2003). We retain the cut-off in the new RMOP opacity codes (Pradhan *et al.* (2023), since the same EOS is employed, but also tested relaxing the cut-off to smaller values up to $w(i) \geqslant 10^{-12}$. However, no significant effect on RMOs was discernible, indicating that a more fundamental revision of (Q)MHD-EOS might be necessary (Trampedach *et al.* (2006). Level population fractions are normalized to unity, and therefore including more levels would not necessarily affect opacities in a systematic manner, as discussed in the next section. unless they are modified with inclusion of possibly missing atomic-plasma microphysics of individual levels and associated atomic data.

4 RESULTS AND DISCUSSION

The EOS determines the contribution to opacity and its cut-off from an atomic level i via the occupation probability $w(i)$ depending on density and resulting plasma microfield, and the level population $pop(i)$ via the Boltzmann factor $exp(-E_i/kT)$ at temperature T. Fig. 1 illustrates the behavior of the EOS parameters for Fe XVII at BCZ conditions. The new RMOP data include autoionizing resonances due to several hundred coupled levels, but can not be directly compared with DW bound-free cross sections that neglect channel coupling and are feature-less (Nahar *et al.* (2023); Zhao *et al.* (2023). However, a comparison of the total monochromatic opacity spectrum can be done to illustrate differences due to plasma broadening of resonances in the RMOP data vs. lines as in the OP DW data.

The primary focus of this work is the interface of EOS with atomic data. As exemplar of the detailed analysis of EOS parameters, Fig. 1 shows the occupation probabilities for Fe XVII at BCZ conditions (red dots, top panel) for all levels with $w(i) > 0.001$, and corresponding level populations (black open circles, middle panel). Since the contribution to RMO is limited by significant level populations $Pop(i)$, the number of levels with $Pop(i) > 0.1\%$ is found to be much smaller, around 50 or so (blue dots, bottom panel). The reason for the given distribution of $w(i)$ (top panel) is because the BPRM calculations are carried out according to total angular momentum quantum number and parity $J\pi$. Therefore, all BPRM data are produced in order of ascending order in energy *within each* $J\pi$ *symmetry*, and descending order due to Stark ionization and dissolution of levels (Mihalas *et al.* (1988).

Tables 1 and 2 give sample RMOs computed at BCZ and Sandia Z temperatures and densities respectively, varying the number of contributing levels NLEV for each of the three Fe ions, and both the MHD and QMHD EOS. Correspondingly, an illustration of RMO behavior is shown in Fig. 2. There is considerable variation in RMO values for small NLEV as expected. The RMOs are very high if all the population is in the ground stae or the first few excited states, but decreasing with NLEV. But then the RMOs approach near-constant values for NLEV ≈ NMAX = 200, for all three Fe ions and for both the MHD and QMHD; no further significant contribution to RMOs is made due to EOS cut-offs and saturation. *Therefore, this 'convergence' should be treated as apparent, and would be real if and only if the EOS is precisely determined.* The converged RMOs should be regarded as a lower bound, in case revisions to EOS enable contributions from more levels that are included in the extensive RMOP atomic datasets, and the EOS+data combination may yield higher opacities.

Table 1. Convergence of the Rosseland Mean Opacity (cm^2/g) with QMHD and MHD equation-of-state for $T = 2\times10^6 K, N_e = 10^{23} cc$. NLEV = number of bound levels in EOS calculations, and NMAX = maximum number of bound levels in R-matrix atomic calculations.

	Fe XVII		Fe XVIII		Fe XIX	
NLEV	QMHD	MHD	QMHD	MHD	QMHD	MHD
1	873.4	891.9	0.92	1.0	69.1	75.6
10	831.0	844.4	324.8	365.5	55.2	60.3
50	225.9	230.3	357.3	392.0	56.8	62.1
100	265.5	270.3	136.8	150.1	23.1	25.3
200	346.5	352.5	175.3	192.4	10.7	11.7
300	360.4	366.6	145.5	159.6	13.9	15.3
500	-	-	169.2	185.7	15.5	16.6
700	-	-	189.4	207.9	12.5	13.7
1000	-	-	197.9	217.2	-	-
Converged RMOs with NLEV = NMAX						
587	352.6	358.7	-	-	-	-
1591	-	-	196.5	215.6	-	-
899	-	-	-	-	12.5	13.7

Table 2. Convergence of RMOs (cm^2/g) with QMHD-EOS and MHD-EOS at Sandia Z $T = 2.11\times10^6 K, N_e = 3.16\times10^{22} cc$.

	Fe XVII		Fe XVIII		Fe XIX	
NLEV	QMHD	MHD	QMHD	MHD	QMHD	MHD
1	456.4	440.0	1.60	1.64	419.2	431.1
10	419.8	403.0	586.6	602.0	334.8	344.0
50	111.2	107.9	654.0	670.9	351.2	361.4
100	129.0	124.1	246.4	252.8	154.4	159.0
200	156.9	150.9	323.7	332.0	82.6	85.0
300	152.8	147.0	267.9	274.9	107.5	110.7
500	142.1	136.7	315.5	323.6	117.7	121.2
700	-	-	351.6	360.7	96.0	98.7
1000	-	-	374.0	374.0	-	-
Converged RMOs with NLEV = NMAX						
587	140.0	134.7	-	-	-	-
1591	-	-	361.6	370.9	-	-
899	-	-	-	-	94.0	96.7

Fig. 3 shows a comparison of the new RMOP opacity spectrum (red) with OP (black). The Sandia Z measurements are also shown (cyan), but it should be noted that the experimental values are convolved over instrument resolution and the magnitudes of individual features are not directly compatible. In the top panel in Fig. 3 the monochromatic opacities are plotted on a $\log_{10}$-scale, and on a linear scale in the bottom panel to better elucidate the differences. The RMOP and OP opacity spectra differ in detailed energy distribution and magnitude. In general, the RMOP background is higher and the peaks lower than OP due to opacity re-distribution, with significant enhancement around 0.7

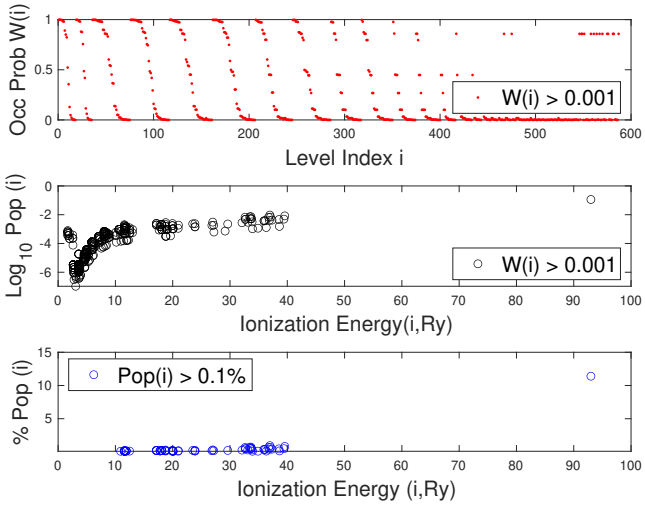

Figure 1. Fe XVII EOS parameters at BCZ conditions: occupation probabilities w(i) as function of level index i (top, red dots); Log_{10} of level populations $Pop(i)$ vs. ionization energy (middle, black open circles); levels with percentage $Pop(i) > 0.1\%$ vs. ionization energy. The ground state population is 11% and the ionization energy is 93 Ry. The $w(i)$ (top panel) correspond to levels i computed along spin-orbital-parity SLJπ symmetries of bound levels in RMOP computations (see text).

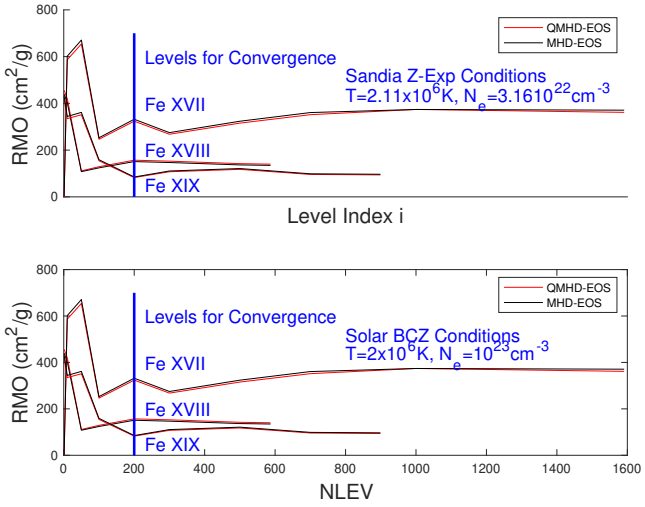

Figure 2. Rosseland Mean Opacity vs. number of levels included in RMOP opacity computations for BCZ and Sandia Z conditions. RMOs appear to 'converge' to constant values around NLEV $\approx$ 200 (however, see text).

keV. The difference is more striking on a linear-scale in Fig. 3 (bottom panel) around 0.9-1.0 keV, where the RMOP peaks are lower by several factors.

Fig. 3 also shows that the Sandia Z measurements span only a small energy range relative to the Planck function derivative dB/dT that determines the Rosseland window and therefore the RMO. But the considerable difference between the background RMOP opacity with experiment remains as with the earlier OP and other works (Bailey *et al.* (2015); Nahar and Pradhan (2016). As we expect, the background non-resonant R-matrix photoionization cross sections are similar to DW results. However, the RMOP results

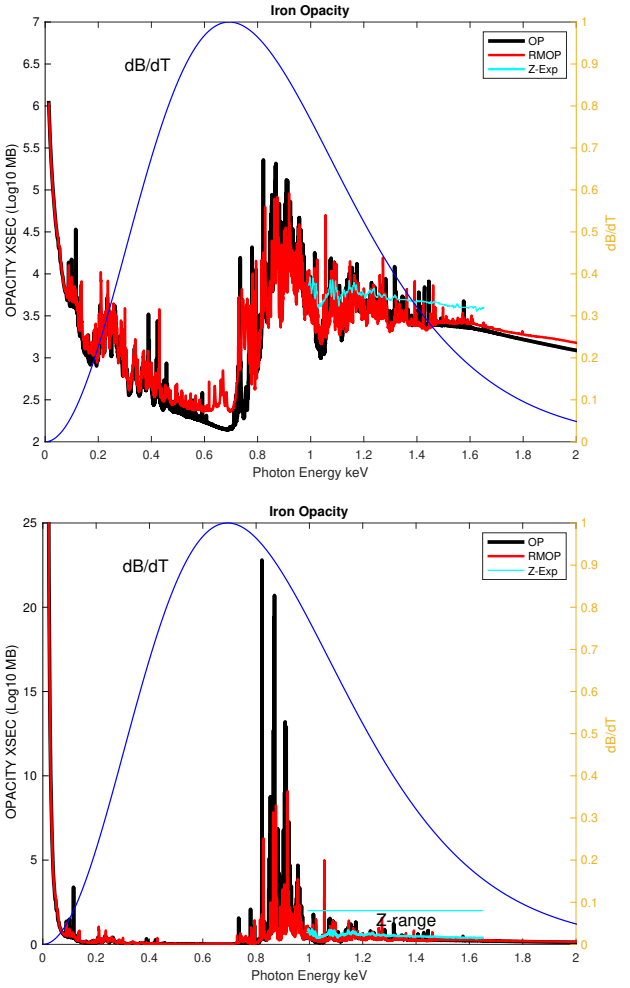

Figure 3. Monochromatic opacity spectra from RMOP, OP and Sandia Z, Log_{10}-scale (top) and linear values x 10^{-4}; the range of the Planck function dB/dT in the Rosseland integrand is also shown. The RMOP results demonstrate redistribution of opacity due to plasma broadening of resonances in the bound free much more than the OP DW data. Except the background, relative magnitude of experimental and theoretical data are not directly comprable since the latter are not convolved over intrumental resolution.

are qualitatively in better agreement with experimental results with shallower "windows" in opacity than OP, for example at $E \approx 1.0$ keV (top panel) and several other energies. Nevertheless, there seems to be a source of background opacity in the Z experiment for iron (Nagayama *et al.* (2019) that is not considered in theoretical calculations.

It is also interesting to revisit the only available comparison between and OP and OPAL occupations probabilities for the simple case of H-like C^{5+} (Badnell and Seaton (2003). Table 3 gives these parameters, and also the level populations going up to $n = 6$. However, owing to the fact that the ground state population dominates over all other levels, and Carbon is fully ionized or H-like at given temperature-density, the RMO remains nearly constant at 170.3 cm^2/g. We might expect similar behavior for Oxygen opacity, though more detailed study is needed, and of course for complex ions such as in this *Letter*.

Table 3. Occupation probabilities w_n and level populations n-pop for H-like C^{5+} at $T = 10^6$ K, $N_e = 10^{22}$ cc. OP opacity calculations neglect all levels with $w_n < 10^{-3}$. Carbon is mostly fully ionized or H-like at specified T,N_e: f(C^{6+}) = 0.431 and f(C^{5+}) = 0.492. RMOs are independent of EOS, ≈ 170 cm^2/g up to any level(s) included.

n	w_n(QMHD)	w_n(MHD)	w_n (OPAL)	Pop(n,MHD)
1	1.00	1.00	1.00	0.438
2	0.997	0.983	0.996	2.42(-2)
3	0.967	0.821	0.995	2.07(-2)
4	0.705	0.249	0.995	8.45(-3)
5	0.154	1.45(-3)	0.914	6.79(-5)
6	1.58(-2)	6.0(-11)	0.527	3.76(-12)

5 CONCLUSION

Whereas improved opacities may now be computed with high precision atomic data using the state-of-the-art R-matrix method, the EOS remains a source of uncertainty. Therefore, the results presented herein should be considered tentative, pending more studies and comparison of (Q)MHD-EOS parameters with other equations-of-state, as well as newly improved versions (Trampedach *et al.* (2006). However, preliminary RMOP results indicate considerable differences with OP iron opacity spectrum, and by extension other existing opacity models based on the DW method and plasma broadening treatment of lines vs. resonances. While the present RMOP iron opacities are significantly higher than the OP owing to higher accuracy and enhanced redistribution of resonance strengths in bound-free opacity, final results might yet depend on an improved MHD-EOS resolving issues outlined herein and related to pseudo bound-free continua (Däppen *et al.* (1987); Seaton *et al.* (1994). Although the contribution may be relatively small around BCZ, completeness requires R-matrix calculations for other Fe ions (in progress). It is also noted that the Sandia Z experimental data are in a relatively small energy range and therefore inconclusive as to determination of RMOs. Although differences in background opacity with experimental data remain unexplained, there appears to be better agreement in detailed features. Finally, the atomic-plasma issues described in this *Letter* need to be resolved accurately in order to obtain astrophysical opacities to solve the outstanding solar problem.

ACKNOWLEDGMENTS

I would like to thank Sultana Nahar for atomic data for Fe ions and discussions. The computational work was carried out at the Ohio Supercomputer Center in Columbus Ohio, and the Unity cluster in the College of Arts and Sciences at the Ohio State University.

DATA AVAILABILITY

The data presented herein are available upon request from the author.

REFERENCES

Christensen-Dalsgaard, J., Däppen, W., Leberton, 2009, Nature 336, 634 (2009)
Basu, S. and Antia, A.M., 2008, Phys. Repts., 457, 217
Basu, S., Grevesse, N., Mathis. S., Turck-Chieze, S., 2015, Space Sci. Rev. 196, 49
Asplund, M., Grevesse, N., Jacques Sauval, A. and Scott, P., 2009, Ann. Rev. Astron. Astrophys. 209, 47
Asplund, M., Amarsi, A.M. and Grevesse, N., 2021, *Astron. Astrophys.* 653, A141
Buldgen, G., Eggenberger, P., Noels, A., Scuflaire, R., Amarsi, A.M., Grevesse, N. and Salmon, S., 2023, *Astron. Astrophys.* 669, L9
Pietrow, A.G.M., Hoppe, R., Bergemann, M. and Calvo, F., 2023, *Astron. Astrophys.* 672 L6
Li, W., Jönsson, Amarsi, A.M. and Grumer, J., 2023, *Astron. Astrophys.* 674, A54
Carlos, M. *et al.* , 2019, *Mon. Not. R. astr. Soc.* 485, 4052
Bailey, J. *et al.* , 2015, Nature, 517, 36
Perry, T. *et al.* , 2018, Proc. *Workshop on Astrophysical Opacities*, PASP 515, 115
Nagayama, T. *et al.* , 2019, *Phys. Rev. Lett.* 122, 235001
Buldgen, G., Jerome, B., Roxburgh, I.W., Vorontosov, S.V. and Reese, D.R., 2022, Frontiers in Astronomy and Space Sciences, 9, 1
Buldgen, G., Noels, A., Baturin, V.A., Oreshina, A.V., Ayukov, S.V., Scuflaire, R., Amarsi, A.M., Grevesse, N., 2023b, *Astron. Astrophys.* (in press)
A.K. Pradhan, S.N. Nahar and W. Eissner, (2023, submitted)
Nahar, S.N., Zhao, L., Eissner, W. and Pradhan, A.K. (2023, submitted)
Pradhan, A.K. (2023, submitted)
Zhao, L., Nahar, S.N., Pradhan, A.K. (2023, submitted)
Nahar, S.N. and Pradhan, A.K., 2016, *Phys. Rev. Lett.* 116, 235003; Ibid., *Phys. Rev. Lett.* 117, 249502
Mihalas, D., Hummer, D.G., and Däppen, W., 1988, *Astrophys. J.* 331, 815
Nayfonov, A., Däppen, W., Hummer, D.G. and Mihalas, D., 1999, *Astrophys. J.* 526, 451
Seaton, M.J., Yu, Y., Mihalas, D. and Pradhan, A.K. (SYMP, 1994), *Mon. Not. R. astr. Soc.* 266, 805
The Opacity Project, The Opacity Project Team, 1995, Vol.1 IOP Publishing Bristol
Seaton, M.J., 2003, OPCD with OP opacities
Mendoza, C. *et al.* , 2007, *Mon. Not. R. astr. Soc.* 378, 1031
Delahaye, F., Badnell, N.R. and Ballance, C.P., 2021, *Mon. Not. R. astr. Soc.* 508, 421
Badnell, N.R. and Seaton, M.J., 2003, *J. Phys. B* 36, 4367
Hummer, D.G., Berrington, K.A., Eissner, W., Pradhan, A.K., Saraph, H.E. and Tully, J.A., 1993, *Astron. Astrophys.* 279, 298
Trampedach, R., Däppen, W. and Baturin, V.A., 2006, *Astrophys. J.* , 646, 560
Pradhan, A.K. and Nahar, S.N., 2011, *Atomic Astrophysics and Spectroscopy* Cambridge University Press
Däppen, W., Anderson, L. and Mihalas, D., 1987, *Astrophys. J.* 319, 195